文章编号: 1001－2060(2008)04－0387－04

大颗粒振动流化床与水平管平均传热特性研究

朱学军, 叶世超, 石进霞, 杨冰释
(四川大学 化工学院, 四川 成都 610065)

摘　要: 在二维流化床(240 mm×80 mm)中, 以平均粒径 d_p 为 0.71、1.83 mm 的玻璃珠和 1.66 mm 的小米为物料, 研究了振动流化床与浸没水平管间传热规律; 考察了气速、振动频率、床高和水平管管径等因素对平均传热系数的影响。结果表明: 随着振动频率的增加最佳的气速可以降低, 随着气速的增加最佳振动频率同样可以降低; 平均传热系数随颗粒粒径减小而增加; 颗粒热物理性质和管径对平均传热系数也有较大影响。通过实验数据得到了计算平均传热系数的关联式, 计算值与实验值吻合较好, 误差在±10%范围内。结果可为带浸没水平管的振动流化床设计和研究提供参考。

关　键　词: 振动流化床; 平均传热系数; 颗粒物性; 最小流化速度
中图分类号: TQ021.3　　文献标识码: A

引　言

带浸没换热管的流化床由于床层温度均一, 传热速率快, 装置尺寸小, 现已广泛用于: (1) 流化床燃烧器, 用来燃烧高硫煤和劣质煤等, 可以有效减少废气排放[1~2]; (2) 流化床反应器, 床层温度易于控制, 有利于催化剂的活化再生[3~4]; (3) 流化床干燥器, 可以实现对块状、颗粒状、膏糊状和液状物料的高效节能干燥[5~7]。

国内外许多学者对不施加振动的流化床与浸没换热管间的传热特性研究较多, 其床料大多为小颗粒, 其颗粒平均粒径小于 1 mm, 主要是基于前面提出的前两种工业应用[8~13], 对于大颗粒研究较少, 而大颗粒和小颗粒其动力学行为具有很大的差异, 颗粒动力学行为在很大程度上影响颗粒的传热特性, 因此对于大颗粒和小颗粒其传热特性也会有较大差别, 通过小颗粒关联出的传热系数就不能用在大颗粒上, 同时将机械振动作用于流化床可以改善气固接触和流化行为, 降低流化床临界流化速度和床层压降, 强化传热传质[14~15]。有关振动流化床与浸没水平管之间的传热特性研究还很少, 所以研究振动流化床浸没加热管与床层传热特性具有重大的理论意义和实际意义。本文以玻璃珠和小米为物料, 研究了大颗粒振动流化床与浸没水平管传热规律, 考察了气速、振动频率、床高和水平管直径等因素对传热的影响。

1　实验装置及流程

振动流化床与水平管局部传热实验装置如图 1 所示, 横截面积为 240 mm×80 mm 的二维流化床由有机玻璃制成, 以便观察物料的流化状态, 气体分布板的开孔率为 4.9%, 孔径 2 mm, 其上铺层不锈钢丝网, 以获得更加均匀的气体分布。床体通过 4 根金属螺旋弹簧被支撑在支架上, 借助偏心机构的作用使之产生竖直方向的正弦振动, 振幅可以通过偏心距来调节, 振动频率通过改变调速电机的转速进行控制。测量传热系数的水平管如图 2 所示, 在直径 25 mm、长 60 mm 的铜棒同心嵌入一长为 60 mm, 直径为 4 mm 的加热棒, 棒体两端用聚四氟乙烯端头封住, 在铜体表面焊接铜－康铜热电偶, 热电偶引线从表面内侧穿过端头引出。水平管两端固定在床壁上。水平管轴线距气体分布板 60 mm, 对称安装在床的中心位置, 床层温度由安装在水平管下方距气体分布板 20 mm 处的裸露热电偶测定。实验物料的特性列于表 1, 最小流化速度通过压降曲线确定。

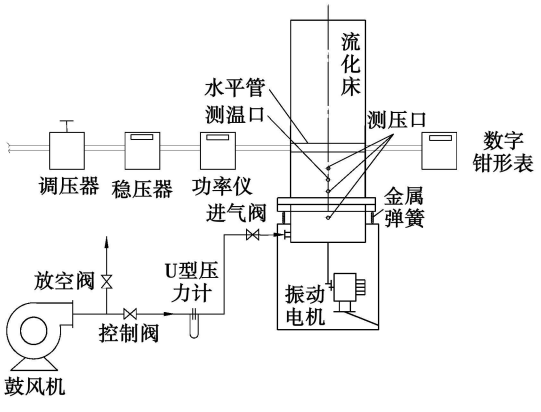

图 1　实验装置流程图

收稿日期: 2007－08－14;　修订日期: 2007－11－12
作者简介: 朱学军(1974－), 男, 四川射洪人, 四川大学博士研究生, 攀枝花学院副教授。

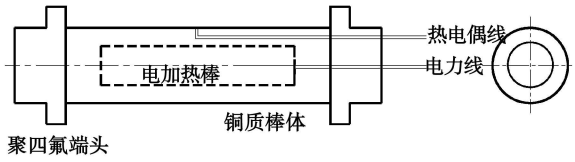

图 2 平均传热系数测试探头

表 1 实验物料特性

	$\bar{d}_p$/mm	ρ_s/kg·m^{-3}	ρ_B/kg·m^{-3}	ε_0	u_{mf}/m·s^{-1}
玻璃珠	0.71	2 500	1 415	0.434 0	0.342 3
玻璃珠	1.83	2 500	1 520	0.392 0	1.159 1
小米	1.66	1 300	835	0.357 7	0.351 0

实验时, 将流化气速调节至一定值, 并使流化床按一定的振幅和频率进行振动, 接通加热电源, 实验持续到微元面的温度稳定不变时, 测得微元管壁温度和床层温度, 即可按下式计算平均传热系数 h:

$$h=\frac{Q}{A_w(t_w-t_B)} \tag{1}$$

式中: h —传热系数, W/(m^2·K); Q—通入水平管的热量, J/s; A—水平管测试部位面积, m^2; t_w—管壁温度, ℃; t_B—床层温度, ℃。

2 实验结果与讨论

2.1 不同振动频率时气速对平均传热系数的影响

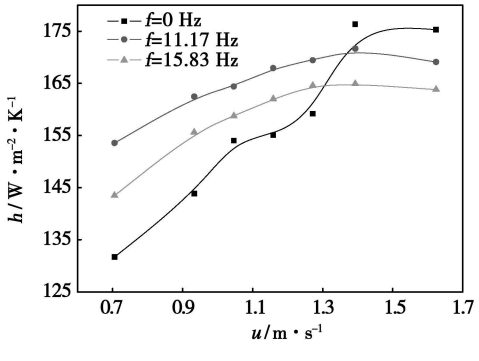

图 3 不同振动频率时平均传热系数与气速关系

图 3 示出了平均颗粒直径为 1.83 mm 的玻璃珠在不同振动频率下平均传热系数随气速的变化情况。由图可见, 平均传热系数随着气速的增加先有一个加速增大的阶段, 然后是一个相对平缓区, 当气速超过一定值, 平均传热系数逐渐减小。这主要由于在某一振动下, 气速较小时, 床层未流化, 相当于固定床传热, 所以传热系数较小。当适当增加气速, 床层开始流化, 传热系数迅速提高, 再增加气速, 气体对流传热变大, 颗粒运动加快, 在表面更新加快, 传热强化, 但速度加大床内颗粒浓度变小, 颗粒对流削弱, 所以中间有一平缓期; 当再增大气速, 颗粒浓度变小, 管壁与气泡接触机会增大成为控制因素, 所以传热系数下降。从图中还可以看出, 振动可以强化传热, 适度增大振动频率, 传热系数增大, 而且达到最大传热系数所需的气速相应变小, 但当振动频率为 15.83 Hz 时, 传热系数反而下降, 主要由于振动过大, 颗粒在管壁上抛掷速度加快, 气泡与管壁的接触时间分率增加, 传热系数因此降低。

2.2 不同气速下振动对传热系数的影响

图 4 示出了平均颗粒直径为 1.83 mm 的玻璃珠在不同气速下传热系数随振动频率的变化情况。由图可见, 低气速下, 传热系数随振动频率增加先增大后减小, 当气速超过一定值后, 传热系数随振动频率增加持续降低。这主要由于低速下, 颗粒未流化, 传热系数较小, 施加一定的振动后, 床层开始流化, 传热系数迅速增加。当振动太强, 床层过度流化, 传热速率下降, 传热系数降低; 当气速超过固定式流化床最小流化速度后, 不加振动, 床层已很好流化, 加振动后, 使管壁处颗粒更新变快, 一方面强化传热, 但另一方面管壁与气泡接触分率增加, 由此削弱传热; 当气速较低时(如图中 u=1.159 1 m/s 时), 前者为控制因素, 传热系数先有一个增加的过程; 当气速达到 1.623 9 m/s, 时后者为控制因素, 传热系数一直降低。

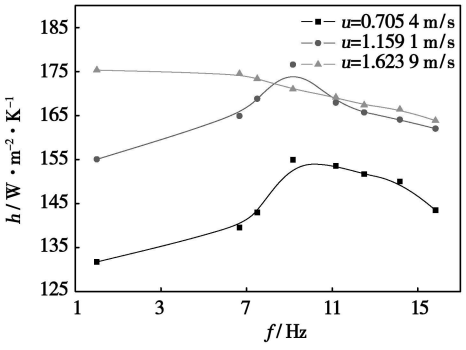

图 4 不同流化速度下平均传热系数与振动频率的关系

2.3 颗粒直径对局部传热系数的影响

图 5 示出了平均颗粒直径为 1.83 和 0.71 mm 的玻璃珠在流化数 N=1 的条件下传热系数随振动频率的变化情况。如图所示, 传热系数随粒径的减小而增大, 主要由于小颗粒与管壁有更多的传热接触点, 接触面积较大, 颗粒对流作用强, 同时小颗粒与管壁间的空隙较小, 气膜厚度较小, 热阻较小, 所以传热系数大。从图中还可以看出对于流化数为 1 时大颗粒在振动频率为 9.2 左右达到最大传热系数, 而对于小颗粒振动频率为 7.5 左右就能获得最大传热系数, 说明振动对小颗粒更敏感一些, 而对于

大颗粒振动能量在床内衰减要快一些。

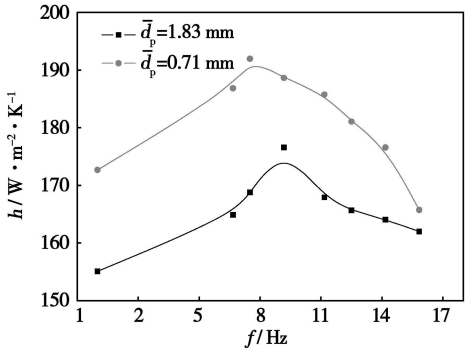

图 5　不同颗粒直径下平均传热系数随振动频率的变化关系

2.4　不同种类颗粒对局部传热系数的影响

图 6 示出了平均颗粒直径为 1.83 mm 的玻璃珠和平均粒径为 1.66 mm 的小米在流化数为 1 的条件下传热系数随振动频率的变化情况。如图所示, 玻璃珠的传热系数要大于小米的传热系数, 这主要是由于玻璃珠的密度大于小米的密度, 相同流化数下玻璃珠的气速要大一些, 其气体对流传热要强一些, 同时玻璃珠和小米的热物理性质的差异, 玻璃珠的导热系数和比热比小米大, 所以传热速率快, 相应平均传热系数就大。

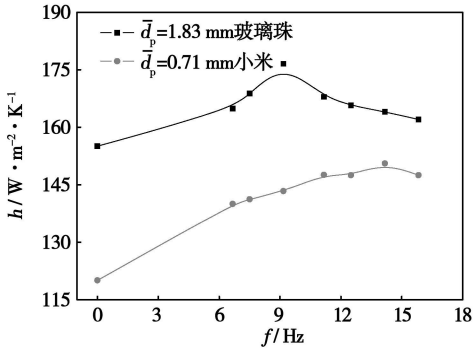

图 6　不同种类物料的平均传热系数随振动频率的变化关系

2.5　床层高度对传热系数的影响

图 7 示出了平均颗粒直径为 1.83 mm 的玻璃珠在临界流化速度时不同床高下传热系数随振动频率的变化情况。如图所示, 两种床高的玻璃珠在同一气速下平均传热系数随振动频率增加均是先增大然后又下降, 在本研究实验条件下, 随着床高的增加, 低振动频率下平均传热系数稍有增加, 高振动频率下平均传热系数稍有变小, 有可能是床高增加后, 床层流化质量变差的缘故。

2.6　管径影响

图 8 示出了平均颗粒直径为 1.83 mm 的玻璃珠在气速为 1.519 1 m/s 下不同管径的水平管与床层间平均传热系数随振动频率的变化情况。由图可见, 在同一气速下, 大管的传热系数要小于小管的传热系数, 而且小管达到最大传热系数需要的振动频率要小于大管。因为在大管背风面更容易形成停滞的粒子帽, 迎风面具有更大的气体空穴, 影响了传热, 而对于较小的管径, 由于振动和气泡的作用使颗粒团在壁面停滞的时间缩短, 从而传热速率快, 传热系数较大。

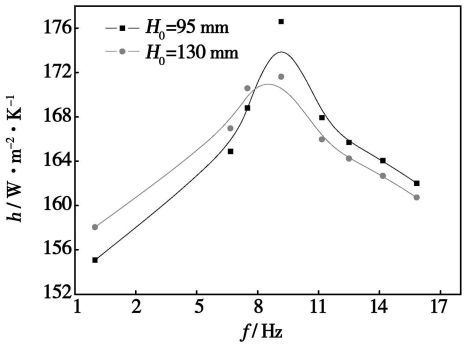

图 7　不同床高下平均传热系数与振动频率的关系 (u= 1.519 1 m/s)

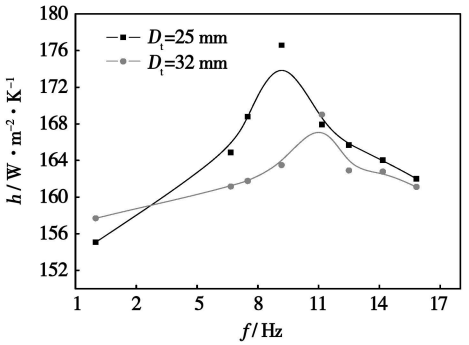

图 8　不同管径下平均传热系数随振动频率的变化关系 (u= 1.519 1 m/s)

2.7　平均传热系数关联式

按量纲分析法, 以实验数据进行多元回归得到平均传热系数的准数关联式:

当 $\Gamma<1$:

$$h=0.461\,5\frac{k_g}{d_p}Re^{0.320\,6}Ar^{0.092\,18}\Gamma^{0.016\,96}\times\left(\frac{H_0}{D}\right)^{-0.048\,33}\left(\frac{D_t}{D}\right)^{-0.255\,5} \tag{2}$$

式中: k_g—气体导热系数, W/(m·K); $\bar{d}_p$—颗粒平均粒径, mm; Re—颗粒雷诺数($=d_p u\rho_g/\mu_g$); Ar—阿基米德数($=d_p^3\rho_g(\rho_s-\rho_g)g/\mu_g^2$); ρ_g—气体密度, kg/m^3; ρ_s—颗粒密度, kg/m^3; u—气速, m/s; Γ—振动强度($=A(2\pi f)^2/g$); A—振幅, mm; f—振动频率, Hz; H_0—静床高度, mm; D—流化床直径, mm; D_t—水平

管直径, mm。各参数的范围: $10 \leqslant Re \leqslant 200$, $Ar \geqslant 2\times 10^5$, $H_0 < 200$ mm, $D_t < 40$ mm(相关系数为 0.964)。

当 $\Gamma \geqslant 1$:

$$h = 0.509\,7 \frac{k_g}{d_p} Re^{0.217\,4} Ar^{0.147\,6} \Gamma^{-0.056\,81} \times \left(\frac{H_0}{D}\right)^{0.039\,26} \left(\frac{D_t}{D}\right)^{-0.084\,24} \tag{3}$$

式中符号的意义和参数的范围同式(2), 相关系数为 0.995 9。

图 9 和图 10 是平均传热系数理论与实验值的比较, 两者吻合较好, 这表明本文提出的平均传热系数关联式是可靠的, 误差在±10%以内。

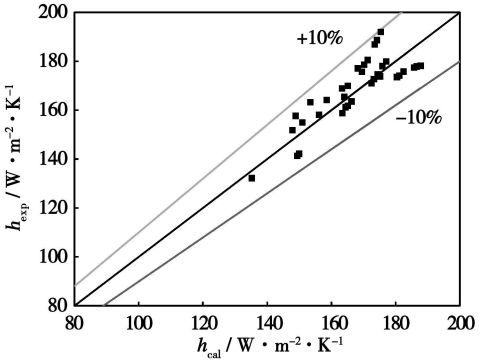

图 9 平均传热系数理论值与实验值的比较($\Gamma < 1$)

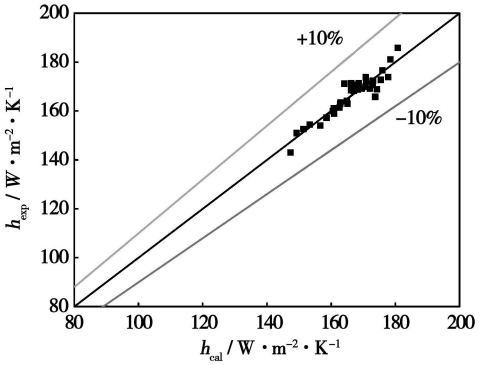

图 10 平均传热系数理论值与实验值的比较($\Gamma > 1$)

3 结 论

(1) 低速下平均传热系数随振动频率的增大先增加后减小, 高气速下随振动频率的增大而降低, 随着气速逐渐加大, 达到最大传热系数的振动频率逐渐降低。同一振动频率下, 平均传热系数随气速的增加先增大后逐渐减小, 振动频率越大, 达到最大传热系数的气速越低。

(2) 颗粒直径越小, 平均传热系数越大, 在同一流化数下, 达到最大传热系数需要的振动频率越低。颗粒的热物理性质对传热有重要影响, 对于粒径大小相差不大的颗粒, 其导热系数越大, 传热系数越大, 比热越高, 传热越强。

(3) 一定静床高度下, 随着床层高度增加, 低振动频率下平均传热系数增加, 高振动频率下平均传热系数降低。

(4) 在同一气速下, 大管的传热系数要小于小管的传热系数, 而且小管达到最大传热系数需要的振动频率要小于大管。

(5) 提出了计算平均传热系数的准数关联式, 在本实验范围内, 计算值与实验值吻合较好。

参考文献:

[1] 林宗虎, 魏敦崧, 安恩科. 循环流化床锅炉[M]. 北京: 化学工业出版社, 2004.

[2] GREWAL N S. A generalized correlation for heat transfer between a gas-solid fluidized bed of small particles and an immersed staggered array of horizontal tubes[J]. Powder Technology, 1981, 30(2): 145—154.

[3] KUNII D, LEVENSPIEL O. Fluidization engineering[M]. New York: John Wiley & Sons, Inc, 1969.

[4] DAVIDSON J F, HARRISON D. Fluidization[M]. London: Academic Press, 1971.

[5] 叶世超. 振动流化床水平换热管传热特性研究[D]. 成都: 四川大学, 2000.

[6] 朱学军, 吕 芹, 叶世超. 惰性粒子振动流化床干燥膏状物料实验研究[J]. 化工学报, 2007, 58(7): 1663—1669.

[7] KUTSAKOVA V E. Drying of liquid and pasty products in a modified spouted bed of inert particles [J]. Drying Technology, 2004, 22(10): 2343—2350.

[8] GREWAL N S. Heat transfer between immersed horizontal tubes and bubbling fluidized beds [J]. Trends in Chemical Engineering, 1994, 2(1): 33—58.

[9] JIM S W, AHN J Y, KIM S D, et al. Heat transfer and bubble characteristics in a fluidized bed with immersed horizontal tube bundle[J]. International of Heat and Mass Transfer, 2003, 46(4): 399—409.

[10] AL BUSOUL M A, ABU EIN S K. Local heat transfer coefficients around a horizontal heated tube immersed in a gas fluidized bed[J]. Heat and Mass Transfer, 2003, 39(5): 355—358.

[11] RASOULI S, GOLRIZ M R, HAMIDI A A. Effect of annular fins on heat transfer of a horizontal immersed tube in bubbling fluidized beds [J]. Power Technology, 2005, 154(5): 9—13.

[12] SCHMIDT A, RENZ U. Numerical prediction of heat transfer between a bubbling fluidized bed and an immersed tube bubbles [J]. Heat Mass Transfer, 2005, 41(4): 257—270.

[13] BEEBY C, POTTER O E. Heat transfer between a horizontal tube bundles and fine particles with air or steam [J]. AIChE Journal, 1984, 30(6): 977—980.

[14] 朱学军, 吕 芹, 叶世超. 振动流化床临界流化速度理论预测与实验研究[J]. 高校化学工程学报, 2007, 21(1): 59—63.

[15] MAWATARI Y, TSUNEKAWA M, TATEMOTO Y, et al. Favorable vibrated fluidization conditions for cohesive fine particles [J]. Power Technology, 2005, 154(5): 54—60.

(编辑 滨)

of Electro-mechanical Engineering, Beijing University of Chemical Technology, Beijing, China, Post Code: 100029), CHEN Sheng-li (Xi' an Thermodynamics Academy Co. Ltd., Xi' an, China, Post Code: 710032)// Journal of Engineering for Thermal Energy &Power. — 2008, 23(4). —378 ~381

Current urgent demands for energy-saving and consumption reduction were described along with the technical theory of a rotor-assembly type intensified heat-transfer device—"Clean-energy Core". The above device has been installed on the 2 # turbo-generator unit of Datang Jiamusze No.2 Power Plant. The condenser at one side of the turbo-generator unit was provided with the device in question while the condenser at another side of the unit was not. The performance test content, testing method and the calculation results of the two condensers of the No.2 power plant were discussed. The performance of the two condensers and the cost-effectiveness of the No.2 unit after installation of the device on one condenser were calculated and analyzed. After the installation of the above-cited device, the terminal temperature difference of the relevant condenser drops by 2.79 ℃, its vacuum increases by 2.97 kPa and its cooling water flow rate decreases by 9.8%. Under the condition of the condensers having the same inlet water temperature and vacuum, the load bearing capacity of the turbo-generator unit will increase by 19.7%, and the water resistance of the condensers increase by 19.52 kPa. The results of the industrial experiments and analytic calculation show that the rotor-assembly type intensified heat-transfer device can be used for condensers in power plants to improve their performance. **Key words**: rotor-assembly type, intensified heat transfer, industrial experiment, turbo-generator unit

平衡目标选择与全息动平衡法的改进研究= **A Study on the Improvement of Balancing Target Selection and Holographic Dynamic Balancing Method**[刊, 汉] / LIAO Yu-he, LANG Gen-feng, QU Liang-sheng (Intelligent Instrument and Monitoring/diagnosis Research Institute, College of Mechanical Engineering, Xi' an Jiaotong University, Xi' an, China, Post Code: 710049)// Journal of Engineering for Thermal Energy &Power. — 2008, 23(4). —382 ~386

Discussed were the problems existing during the description of the balancing state of a rotor by using a working-frequency trajectory initial-phase vector, which serves as a balancing target in a holographic dynamic-balancing method. Through a precession decomposition of the working-frequency trajectory of the rotor, the different influences of the unbalanced mass of the rotor on its positive and reverse precession component were analyzed in detail. It has been shown that the reverse precession component is not a direct reflection of the balancing state of the rotor. Under the condition of a trajectory with a large eccentricity, the interference on the estimation of the unbalanced mass caused by the reverse precession component should not be neglected. On this basis, presented was an improved holographic dynamic-balancing method with the positive-precession component trajectory initial-phase vector of the rotor serving as a balancing target. Under the condition of not influencing the balancing accuracy of the original holographic dynamic-balancing method, the counterweight version calculation process has been simplified. Compared with the traditional balancing methods, the method under discussion is more accurate and effective. On-site practical applications have verified the reliability and validity of the method. **Key words**: rotor, holographic dynamic-balancing, precession, initial phase vector

大颗粒振动流化床与水平管平均传热特性研究= **A Study of the Characteristics of Average Heat Transfer Between a Big-particle Dominated Vibrating Fluidized Bed and Horizontal Tubes**[刊, 汉] / ZHU Xue-jun, YE Shi-chao, SHI Jin-xia, et al (College of Chemical Engineering, Sichuan University, Chengdu, China, Post Code: 610065)// Journal of Engineering for Thermal Energy &Power. — 2008, 23(4). —387 ~390

In a two-dimensional fluidized bed (240 mm× 80 mm), with glass beads of average diameters d_p of 0.71 mm and 1.83 mm and millet of 1.66 mm diameter serving as materials, studied was the heat transfer law between the vibrating fluidized bed and submerged horizontal tubes. The influence of such factors as gas flow speed, vibration frequency, bed height and diameters of horizontal tubes etc. on the average heat transfer coefficient was investigated. The results of the study show that with an increase of the vibration frequency, the optimum gas flow speed will decrease, and with an increase of the gas flow speed, the optimum vibration frequency will also go down. The average heat transfer coefficient will increase with a decrease of the particle diameter. The particle thermo-physical properties and the tube diameter also have a relatively big influence on the average heat transfer coefficient. From the test data, a correlation formula for the calculation of the average heat transfer coefficient has been obtained. The calculation values have been in relatively good agreement with the test ones, and the calculation error is within a range of ±10%. The above results can serve as reference data for the design and study of vibrating fluidized beds fitted with submerged horizontal tubes. **Key words**: vibrating fluidized bed, average

heat transfer coefficient, particle themro-physical property

掺烧石油焦 410 t/h 循环流化床锅炉 NO_x 排放特性研究＝**A Study of NO_x Emission Characteristics of a 410 t/h Circulating Fluidized Bed Boiler Burning a Mixture of Coal and Petroleum Coke**[刊, 汉] / DUAN Lun-bo, ZHAO Chang-sui, LI Ying-jie, et al (Education Ministry Key Laboratory on Clean Coal Power Generation and Combustion Technology, Southeast University, Nanjing, China, Post Code: 210096)// Journal of Engineering for Thermal Energy & Power. — 2008, 23(4). —391 ~394

An experimental study was performed of the influence of operating parameters on NO_x emission characteristics of a 410 t/h circulating fluidized bed boiler burning a mixture of coal and petroleum coke. The law governing the change of NO_x emission concentration with such parameters as temperature, excess air factor, primary air rate and calcium/sulfur ratio etc. was expounded when the boiler burns the following three kinds of fuel: bituminous coal, 70% bituminous coal + 30% petroleum coke, and 50% anthracite + 50% petroleum coke. The results of the study show that when the boiler burns different fuels, its NO_x emission concentration is in positive correlation with fuel volatile content. With an increase in temperature, NO_x emission concentration will increase. The furnace atmosphere exercises an enormous influence on the NO_x emission concentration. With an increase of the excess air factor and primary air rate, NO_x emission concentration will also increase. With an increase of calcium/sulfur molar ratio, NO_x emission concentration will decrease. The test results can well provide practical guidelines for the operation of circulating fluidized bed boilers burning a mixture of coal and petroleum coke. **Key words**: circulating fluidized bed boiler, burning of a mixed fuel, petroleum coke, NO_x emission concentration

基于多模型集的主汽温多模型预测控制方法＝**Main Steam Temperature Multi-model Prediction and Control Method Based on a Multi-model Set**[刊, 汉] / LIU Ji-zhen, YUE Jun-hong, TAN Wen (Automation Department, North China University of Electric Power, Beijing, China, Post Code: 102206)// Journal of Engineering for Thermal Energy & Power. — 2008, 23(4). —395 ~398

Concerning a kind of industrial processes for which first-order inertia plus a pure lagging model can be used to describe their dynamic characteristics under different operating conditions and which change with operating conditions, a method was presented for setting up a multi-model set based on the maximum and minimum values of the characteristic parameters of an object. A recursive Bayesian probability weighting method was used to obtain an overall predictive model. On this basis, a multi-model predictive controller was designed to meet the control requirement for the operating conditions varying in a wide range. In the meanwhile, when a rectification of errors is being performed, the prediction error of the model resulting from any dynamic change of the operating condition can be compensated in advance to enhance prediction accuracy. The simulation calculation results of a utility boiler main steam temperature system show that the method under discussion enjoys a superior ability to track a set value under various operating conditions. When the operating conditions change in a wide range, it is possible to stabilize the main steam temperature near a set value. **Key words**: main steam temperature system, multi-model set, multi-model prediction control, Bayesian probability weighting, dynamic feedforward

600 MW 燃煤电站烟气汞形态转化影响因素分析＝**An Analysis of the Factors Exercising an Influence on the Morphological Transformation of Mercury in the Flue Gas of a 600 MW Coal-fired Power Plant**[刊, 汉] / WANG Yun-feng, DUAN Yu-feng, YANG Li-guo, et al (College of Energy Source and Environment, Southeast University, Nanjing, China, Post Code: 210096)// Journal of Engineering for Thermal Energy & Power. — 2008, 23(4). —399 ~403

Mercury emissions from coal-fired power plants are regarded as the largest pollution source of man-made mercury emissions in nature. Hence, to perform an on-the-spot testing of the mercury emission concentration in various forms from a coal-fired power plant is of vital significance for understanding and controlling the law and regularity of mercury emissions. With the internationally accepted Ontario Hydro method being adopted to sample the flue gas before and after an electrostatic precipitator (ESP) in a 600 MW coal-fired power plant, the American EPA (Environmental Protection Agency) standard method was used to determine Hg^0, Hg^{2+} and Hg^P concentration in the flue gas, and DMA 80 was employed to ascertain the mercury concentration in solid samples (coal, bottom ash, ESP fly ash). The testing results show that when the flue gas passes through the ESP, the morphology of the mercury contained in the flue gas will undergo a remark-